JOURNAL OF COLLOID AND INTERFACE SCIENCE 202, 430–440 (1998)
ARTICLE NO. CS985463

Colloidal Charge Determination in Concentrated Liquid Dispersions Using Torsional Resonance Oscillation

J. Bergenholtz,*,[1] N. Willenbacher,* N. J. Wagner,† B. Morrison,* D. van den Ende,‡ and J. Mellema‡

*Polymer Research Division, BASF AG, D-67056 Ludwigshafen, Germany; †Center for Molecular & Engineering Thermodynamics, Department of Chemical Engineering, University of Delaware, Newark, Delaware 19716; and ‡Faculty of Applied Physics, University of Twente, 7500 AE Enschede, The Netherlands

Received October 7, 1997; accepted February 9, 1998.

The high-frequency rheology of concentrated liquid charge-stabilized dispersions has been measured using a surface-loaded torsional resonator. The high-frequency shear moduli are extracted from the measurement as a function of ionic strength and surface acid content. A theory which enables the determination of the effective surface charge of the concentrated dispersions is presented. At high ionic strengths the theory simplifies to an analytic formula relating the effective surface charge to the high-frequency limiting shear modulus in terms of an effective hard-sphere diameter. The effective hard-sphere diameter is obtained experimentally from the high concentration asymptote of the zero-shear viscosity. The resulting effective surface charge increases with added electrolyte content in agreement with charge renormalization theory. The effective charge also increases with added weak and strong surface acid content. The method, which operates on concentrated dispersions, is found to yield effective charges that agree with dilute measurements of the electrophoretic mobility. Moreover, the effective hard-sphere scaling reduces the high-frequency viscosity to a master curve independent of salt content.

Key Words: suspensions; surface charge; charge renormalization; rheology; concentrated dispersions.

INTRODUCTION

The surface charge density of colloidal particles in polar media is an important quantity that often controls colloidal stability (1), phase behavior (1–3), and both static and dynamic properties (4, 5). Much effort has been invested in developing experiments and theoretical treatments directed at the reliable determination of the surface charge or the surface potential. Most of the available methods for determining the surface charge rely on measurements of a single particle response, e.g., electrophoretic mobility (6, 7), or a response averaged over a dilute ensemble of particles, e.g., conductivity (7) or electroacoustic spectroscopy (8). Hence, these methods require operations at low particle concentrations at which the simplified theoretical considerations allow for conversion of the measurement to surface charge or potential. Another simplification sometimes made is using the linearized version of the Poisson–Boltzmann equation in the analysis of various measurements, such as small-angle scattering (9, 10), conductivity (11), and self-diffusion (12). The proviso for using the simpler linear theory is that the bare surface charge must be renormalized, that is, replaced by an effective charge, smaller than the bare charge (13–15). Consequently, discrepancies are found between the charge determined by conductometric titration, which yields the total surface charge, and the effective charge resulting from analyses using the linear Poisson–Boltzmann theory (16). In addition, one expects that the effective charge will show some dependence on the type of measurement used as well as on dispersion properties.

In many cases measurements under dilute conditions are not practically realizable or even desirable. Variation of surface properties with dilution is a concern when the results from dilute measurements are extended to predict the behavior of concentrated dispersions. Also, the detailed composition of the solvent in concentrated industrial dispersions is often unknown. Determination of the surface charge by direct measurement of a concentrated dispersion is an attractive prospect, suggesting the possibility of designing procedures for on-line characterization. It is the purpose of this work to provide a method whereby an effective surface charge can be obtained from a direct measurement of *concentrated* dispersions. We demonstrate how measurements of the elastic shear modulus can be used to obtain the surface charge of concentrated charge-stabilized dispersions. The use of elastic shear moduli to provide information of particle interactions is not a new concept (1, 17–24), but its extension to include concentrated liquid dispersions is. Further, the method presented is general and can be extended to probe other colloidal interactions.

[1] To whom correspondence should be addressed at Department of Physics, University of Konstanz, P.O. Box 5560, D-78457 Konstanz, Germany. E-mail: Johan.Bergenholtz@uni-konstanz.de.

0021-9797/98 $25.00

Colloidal liquids respond essentially as purely viscous materials at low frequencies. They acquire progressively more solid-like character as the frequency is increased, usually leading to a terminal high-frequency response. The response is characterized by high (relative to the inverse structural relaxation time (4, 5)) frequency shear elasticity and viscosity. Statistical mechanics connects the high-frequency shear modulus to the colloidal interaction potential (and the microstructure of the dispersion) (25, 26) and, hence, the surface charge in charge-stabilized dispersions. This has been exploited in the past to study the interactions in dispersions characterized by long relaxation times and/or high elasticity, e.g., crystalline (18–21, 27–29), glassy (17), or flocculated (22, 30) dispersions. These studies employed mechanical spectroscopy, which is well suited to investigations of concentrated colloidal dispersions. The instrumentation used includes shear wave velocity (19–21, 28) and shear wave damping measurements (17, 18, 31, 32), as well as rotational rheometry (23, 24). The measurement of the damping of shear waves can be conducted in the surface loading regime, where it is then sufficiently sensitive to cover the important case of liquid, nonflocculated dispersions, e.g., hard-sphere (33), adhesive hard-sphere (34), sterically stabilized (24), and liquid charge-stabilized dispersions. These types of dispersions also show elasticity, though usually of smaller magnitude than colloidal crystals or flocculated dispersions. Nevertheless, at sufficiently high particle concentrations and frequencies liquid dispersions show a measurable elasticity. We note for completeness that the colloidal surface charge of *concentrated* dispersions can be obtained from the analysis of small-angle neutron scattering (9), a technique of limited availability.

In this work we use high-frequency torsional resonance oscillation to determine elastic shear moduli. Torsional resonance oscillation was developed originally to study the viscoelastic behavior of polymer solutions (35, 36). In this work we employ a particularly simple, commercially available torsional resonator. From the damping of an immersed torsionally oscillating rod we obtain the elastic shear modulus. To convert the measured modulus to a surface charge we use previously derived statistical mechanical expressions, coupled with a perturbation theory for the structure of the concentrated dispersions. At high ionic strength the theory reduces to an analytic formula, relating the elastic shear modulus to the surface charge. The proposed formula is the liquid analogue of a series of relations that have found widespread use for the case of ordered dispersions (23, 26, 28, 37). We test the method on well-characterized polymer dispersions at high concentrations.

In the following, we first describe the model dispersions and the instrumentation used. The theoretical analysis is then presented and the simplifying approximations are stated and analyzed. Results are presented, confirming the sensitivity of the measurement to the colloidal interaction potential. The extracted surface charge is compared to results from conventional techniques for determining the surface charge. The comparison shows that the charge must be interpreted as an effective charge, different from the total charge found using conductometric titration, but in good agreement with that obtained from electrophoretic mobility measurements under dilute conditions.

EXPERIMENTAL

Dispersions

Poly(*n*-butyl-methacrylate) (PBMA) dispersions were prepared by emulsion polymerization using sodium dodecyl sulfate as emulsifier and sodium persulfate as initiator. Some of the dispersions were copolymerized with acrylic acid (PBMA/AA), giving rise to weak ($-COO^-$) in addition to the strong ($-OSO_3^-$) acid surface groups derived from the initiator. Purification of the dispersions proceeded by dialysis against deionized water, followed by ion exchange (Amberlyst IRN-150, Polysciences), and finally dialysis against an electrolyte solution maintained at pH 6 and desired ionic strength. The pH and ionic strength were regulated by addition of HCl/KOH (reagent grade, Fluka) and KCl (reagent grade, Fluka). The final dialysis step was often combined with a reverse osmosis step (dialysis under pressure) to obtain more concentrated dispersions (27). This procedure was found to result in lattices with reproducible rheological properties and no drift in conductivity with storage time. The weight fraction of polymer in the dispersions was determined by drying samples *in vacuo* for 24 h at 60°C. The weight fraction was then converted to a particle volume fraction by using the specific volume of the polymer (1.063 g/cm^3), determined using dilution density measurements (Paar DMA40). Concentration series were prepared by diluting the dispersions with the electrolyte solution used as dialysate. This procedure results in a slight variation in the dispersion ionic strength with particle concentration due to the membrane equilibrium that exists between dispersion and dialysate. This effect is accounted for self-consistently in the data analysis.

The particle size was determined by dynamic light scattering. The size polydispersity was obtained from capillary hydrodynamic fractionation (CHDF). The electrophoretic mobility was measured using a Zetasizer 3000 (Malvern) and was converted to an effective charge using Henry's equation (38), neglecting surface conductivity and double-layer distortions. The total analytical surface charge was determined by conductometric titration using NaOH/HCl as titrant. The synthesized particles, their size, initiator content, and titration charges are tabulated in Table 1.

All rheological measurements were conducted at 20°C,

which is below the glass transition temperature of the PBMA particles (~30°C). Zero-shear viscosities were obtained from well-defined low-shear plateaus, found in steady shear measurements using an RFSII rheometer (Rheometrics).

Torsional Resonator

A commercially available torsional resonator (Rheoswing, Physica) with a particularly simple design was used to measure the viscoelastic properties of the dispersions. As shown in Fig. 1, the instrument consists of a torsionally oscillating rod which is immersed in the dispersion. The torsional motion is driven by a piezoelectrically excitable crystal coupled to the rod. The resulting resonance frequency is approximately $\omega_{0,air}/2\pi \approx 8.858$ kHz in air at 20°C. The torsional motion creates a damped shear wave in the liquid medium that propagates a characteristic distance δ (see Fig. 1), given for a plane wave by (35)

$$\delta = \sqrt{\frac{2}{\rho\omega^2}\frac{G'^2 + G''^2}{\sqrt{G'^2 + G''^2} - G'}}, \qquad [1]$$

where ρ is the liquid density, ω is the frequency of oscillation, and G' and G'' are the shear storage and loss moduli, respectively. For water, the solvent used in this study, the typical penetration depth is 6 μm. This value sets the lower boundary on δ for the dispersions. In this study the particle radii are ~40 nm and the shear wave extends at least 15 particle radii into the dispersion. Thus, the bulk dispersion is probed by the instrument. To simplify the analysis we conduct the torsional oscillation in the surface loading limit, meaning that we use a gap width much greater than δ so that no reflections from the sample container wall occur. For the most concentrated dispersions used in this study Eq. [1] yields ~50 μm, which is far smaller than the 1000-μm gap width used.

Another concern is that the measurement be conducted in the linear viscoelastic regime. The angular amplitude of the torsional motion cannot be monitored or controlled using the Rheoswing torsional resonator; therefore, we use an indirect means of assessing whether the measurements are in the linear regime. The maximum strain imposed on the liquid by a plane propagating wave is given by

$$\gamma_{max} = \dot{\gamma}_{max}/\omega = R\theta_0\sqrt{\frac{\rho\omega^2}{\sqrt{G'^2 + G''^2}}}, \qquad [2]$$

where θ_0 is the angular displacement amplitude and R is the radius of the torsion rod. The maximum $R\theta_0$ occurs at the rod tip and is at most 50 nm according to the manufacturer (Physica). This estimate yields maximum strains between 0.3 and 1% for the most and least viscoelastic dispersions in this study, respectively. Typical colloidal liquids show linear viscoelasticity when the strain is kept below 1% (39). Moreover, the linear regime broadens as the frequency of the measurement is increased (39). Thus, for the frequencies of interest here, the linear viscoelastic regime is being probed.

When the rod is immersed in a liquid, its motion is damped due to the liquid's impedance. This leads to a broadening of the resonance curve ($\Delta\omega$) and a lowering of the resonance frequency (ω_0) compared to a measurement in air. Both of these effects are characteristic of the surrounding liquid, as the motion of the rod depends on the liquid deformation and hence the viscoelastic properties of the liquid. The real and imaginary parts of the liquid impedance $Z = R + iX$ are related to the damping and frequency shift, respectively (35, 40),

$$R = K_1(\Delta\omega - \Delta\omega_{air})$$
$$X = K_2(\omega_{0,air} - \omega_0), \qquad [3]$$

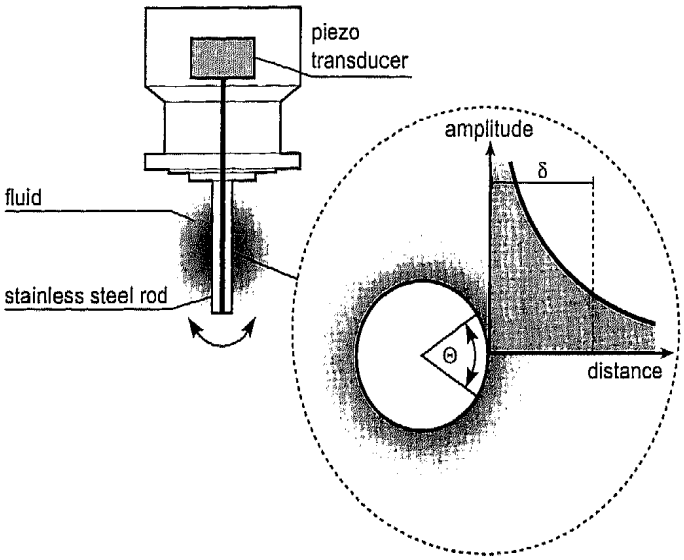

FIG. 1. Schematic drawing of the Rheoswing torsional resonator. Also shown is the penetration depth δ, which is the characteristic radial distance that the shear wave propagates away from the torsional rod.

TABLE 1

Characterization of Polymer Lattices: Particle Type, Particle Radius (a), Size Polydispersity (s_a/a), Weight Percentage Initiator, and Titrated Charge Density

Particle type	a (nm)	s_a/a	NaPS (wt %)	$q_{titration}$ (μC/cm^2)
PBMA/AA	43.5	0.14	0.40	30.7[a]
PBMA1	38	0.3[b]	0.40	1.56
PBMA2	37	0.12	0.15	1.14
PBMA3	40	0.11	0.67	1.64

[a] This number represents the weak acid surface charge density. No reliable estimate for the strong acid surface charge density could be obtained due to the interference from the weak acid end point [68, 69].

[b] The high polydispersity is caused by a slight bimodality.

where K_1 and K_2 are calibration constants. The Rheoswing's mechanical quality factor $\omega/\Delta\omega$ for water at 20°C is about 2000. As the penetration depth is small in relation to the radius of the torsion rod, we expect that the curvature of the rod will play a minor role. By including the leading order curvature correction (41) in the analysis we have verified that $Z = Z_{pl}$ is indeed an excellent approximation for the Rheoswing. Here $Z_{pl} = R_{pl} + iX_{pl}$ is the mechanical impedance of a planar wave front in the surface loading limit. The components of the shear modulus are related to Z_{pl} via

$$G' = (R_{pl}^2 - X_{pl}^2)/\rho$$
$$G'' = (2R_{pl}X_{pl})/\rho. \quad [4]$$

A series of Newtonian liquids, covering the viscosity range $1 < \mu < 80$ mPa·s, were used to calibrate the Rheoswing at 20°C according to Eq. [3]. The calibration constants were found to be $K_1 = 74.17$ and $K_2 = 128.6$ kg/m^2. An ideal resonator would have $K_2 = 2K_1$ (42, 43).

For the ensuing theoretical analysis to be valid, we require that the frequency of oscillation be high enough so that the high-frequency rheology of the dispersions is measured. More specifically, the timescale of diffusive colloidal motion must be long compared to the times probed by the Rheoswing, or, stated equivalently

$$\omega/2\pi \gg D_S^S/l^2. \quad [5]$$

The characteristic frequency D_S^S/l^2 delineates the regime where the structure of the concentrated dispersion can no longer rearrange significantly in response to the oscillatory strain field. It contains the short-time self-diffusion coefficient D_S^S, which is the characteristic small displacement mobility of a colloidal particle in the concentrated dispersion (4, 5), and the mean interparticle separation l. For a dilute dispersion of 40-nm particles, using $D_S^S \approx D_0$, the bare diffusion coefficient, and $l \approx a$ yields a frequency of approximately 3 kHz. This is nearly the resonance frequency of the Rheoswing torsional resonator. Increasing particle concentration will, however, decrease D_S^S strongly, suggesting that the Rheoswing will probe the high-frequency limit at higher particle concentrations. To ensure that the high-frequency condition is achieved, we have performed some measurements over a limited range of frequencies. The ~8.9-kHz Rheoswing measurements were complemented by two additional frequencies obtained from measurements using the electromagnetically driven torsional pendula at the University of Twente. The torsional pendula yielded two additional frequencies: ~685 Hz and 2.33 kHz. The torsional pendula have been described in detail previously (42, 43) and have been shown to yield accurate results for a variety of colloidal dispersions (30, 33, 34). Figure 2 shows the frequency-dependent dynamic viscosity, $\eta' = G''/\omega$, for PBMA dispersions of 40-nm-radius particles as a function of particle volume fraction. The dynamic viscosity is seen to decrease with increasing frequency at all concentrations. This trend results from the decreasing (with increasing frequency) contribution to η' from the interparticle interactions and Brownian motion (1). Though difficult to judge due to the limited frequency range, the data appear to converge to a frequency-independent η'_∞ located at, or close to, the Rheoswing frequency of ~8.9 kHz. When plotted against $\omega^{-1/2}$, the scaling found experimentally by van der Werff *et al.* (33), the dynamic viscosity data decrease sublinearly, indicating convergence to a high-frequency plateau. Also shown in Fig. 2 is a line representing the high-frequency viscosity for hard-sphere dispersions,

$$\eta'_\infty/\mu = \frac{1 + \frac{3}{2}\phi(1 + \phi - 0.189\phi^2)}{1 - \phi(1 + \phi - 0.189\phi^2)}, \quad [6]$$

where ϕ is the particle volume fraction. This semi-empirical formula was constructed by Lionberger and Russel (44, 45) such that the exact dilute and concentrated hard-sphere limits are satisfied. The dynamic viscosities in Fig. 2 lie well above the hard-sphere behavior.

Figure 3 shows the dynamic storage modulus G' for the same set of measurements as displayed in Fig. 2. Again, the Rheoswing data obtained at ~8.9 kHz lie close to the ~2.3-kHz data, indicating that a frequency of 8.9 kHz satisfies the high-frequency requirement represented by Eq. [5].

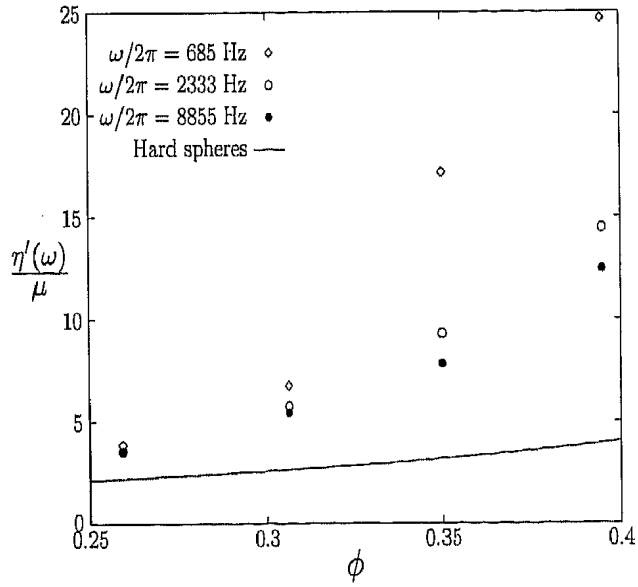

FIG. 2. Dynamic viscosity as a function of volume fraction and frequency for PBMA1: a = 38 nm and [KCl] = 30 mM. The line represents hard-sphere behavior (44).

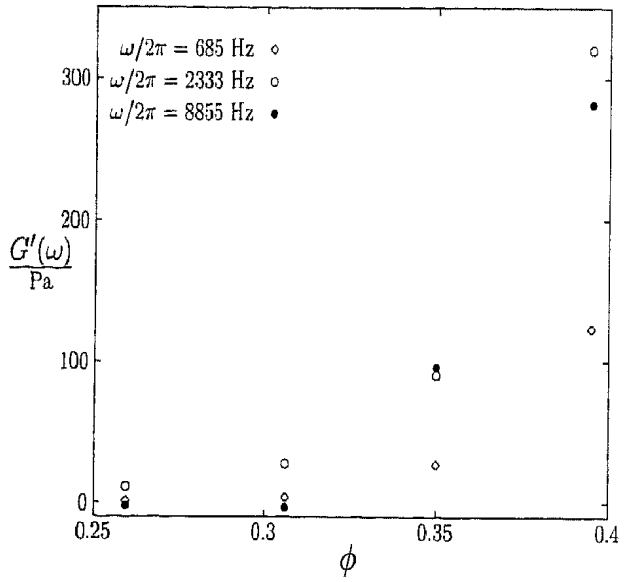

FIG. 3. Dynamic shear modulus as a function of volume fraction and frequency for PBMA1: a = 38 nm and [KCl] = 30 mM.

THEORY

Interaction Potential

When polymer particles are dispersed in a polar medium, they acquire charge due to the dissociation of the acidic surface groups incorporated in the polymerization procedure. The electrostatic potential in the ionic medium surrounding the particle(s) is described by the Poisson–Boltzmann equation. Linearization of the Poisson–Boltzmann equation leads to the analytic Debye–Hückel single-sphere potential. Linear superposition of single-sphere potentials results in an interaction potential (scaled by the temperature kT) of Yukawa form (46)

$$\Psi_{el}(r)/kT = \left(\sqrt{\frac{L_B}{a}}\frac{Qe^{\kappa a}}{1+\kappa a}\right)^2 \frac{e^{-(\kappa a)r}}{r}, \qquad [7]$$

where r is the center-to-center separation distance made dimensionless with the particle radius a. The Yukawa prefactor for particles with constant surface charge Qe contains in addition the Bjerrum length $L_B = e^2/4\pi\epsilon kT$ (with e the elementary charge and ϵ the dielectric constant of the medium) and the inverse Debye length κa. The inverse Debye length, here made dimensionless with a, gauges the extent of the electrical double layer and is, for a monovalent electrolyte, given by

$$(\kappa a)^2 = 4\pi a^2 L_B\left(\frac{n_+}{1-\phi}+\frac{n_-}{1-\phi}\right), \qquad [8]$$

where $n_\pm$ are the number concentrations of free positive and negative ions in the dispersion including counterions from dissociated surface chemical groups. The inclusion of the factor $(1-\phi)^{-1}$ reflects the reduced volume available to the added electrolyte and counter ions due to the presence of the colloidal particles (1, 47, 48). In this work the dispersions are dialyzed and so the added electrolyte concentrations $n_\pm$ depend on the Donnan membrane equilibrium (49)

$$\frac{n_\pm}{1-\phi} = \mp\frac{Qn_{\text{particles}}}{2(1-\phi)} + \sqrt{\left(\frac{Qn_{\text{particles}}}{2(1-\phi)}\right)^2 + n_{\text{salt}}}, \qquad [9]$$

where $n_{\text{particles}}$ and n_{salt} are the number concentrations of colloidal particles in the dispersion and of the salt in the dialysis bath. Equations [8] and [9] together are consistent with the linearized Poisson–Boltzmann theory, as the resulting Debye length is equal to that derived by Russel and Benzing (47). Note that κa is dependent on both the colloid charge Q and the particle volume fraction ϕ through the charge neutrality and excluded volume effect implicit in Eqs. [8] and [9].

The interaction potential in Eq. [7] is taken to describe the electrostatic repulsion between the charged PBMA particles in this study, recognizing that Q is to be interpreted as an effective charge (13–15). In addition to electrostatic repulsion, we superpose the nonretarded, attractive van der Waals free energy of interaction between spheres. The total composite interaction potential assumes now the classical DLVO form (50)

$$\Psi(r) = \Psi_{el}(r) + \Psi_{vdW}(r) \qquad [10]$$

$$\Psi_{vdW} = -\frac{A}{6}\left(\frac{2}{r^2-4}+\frac{2}{r^2}+\ln\left(\frac{r^2-4}{r^2}\right)\right). \qquad [11]$$

We have taken the Hamaker constant $A = 1.05\cdot 10^{-20}$ J, the value for PMMA (1), as an approximation for the PBMA particles. For the small particles in this study the van der Waals contribution to the total interaction potential is small, but not negligible due to the high levels of added electrolyte.

Elastic Modulus

For isotropic molecular fluids with central forces Zwanzig and Mountain (25) derived the relationship between the high-frequency elastic shear modulus G'_∞ and the interaction potential. This expression is given in dimensionless form as

$$G'_\infty\frac{a^3}{kT} = \frac{3\phi}{4\pi} + \frac{3\phi^2}{40\pi}\int_0^\infty drg(r)\frac{d}{dr}\left(r^4\frac{d\Psi(r)/kT}{dr}\right), \qquad [12]$$

where $g(r)$ is the radial distribution function that describes positional correlations among particles in the equilibrium fluid. For colloidal dispersions the same formula results when the hydrodynamic interactions among particles are ne-

glected (26, 44). This hydrodynamic coupling is a secondary effect for the elastic shear modulus (of non-hard-sphere fluids), but is important for dissipative properties such as the shear and high-frequency viscosities. When hydrodynamic interactions are included in the analysis, additional hydrodynamic functions appear that are difficult to evaluate (44, 45, 51). In the present analysis we neglect the hydrodynamic interactions and the starting point is then Eq. [12].

To justify neglecting the hydrodynamic interactions in this particular study, we refer to the computer simulations done by Bossis *et al.* (52) and the scaling analysis done by Lionberger and Russel (44, 45). They have shown that as the particle concentration is increased the long-range nature of the (conditionally averaged) hydrodynamic functions that appear in the expression for the shear modulus is suppressed; that is, the hydrodynamic interactions act mainly in a lubrication region near the particles. As the particles in this study are electrostatically stabilized, this near field region is not likely to be sampled, so it is reasonable to neglect the effect of hydrodynamic interactions on G'_∞ entirely.

In principle, Eq. [12] can be used directly to determine the surface charge; however, solving Eq. [12] for the surface charge requires integration and also iteration. The latter is a consequence of the implicit dependence of the radial distribution function on the interaction potential and accordingly on the surface charge. Moreover, the radial distribution function for non-hard-sphere colloids is generally cumbersome to calculate. We seek to circumvent calculation of the complete radial distribution function and to construct a simplified model based on perturbation theory to provide a direct route for determining the surface charge from a measurement of the elastic shear modulus. Such simple, analytical relations have been obtained for the special case of ordered dispersions assuming that only nearest neighbor particle interactions contribute to the elasticity. For liquid dispersions particle positions are not as strongly localized and the characteristic disordered structure must be taken into account. As shown in the Appendix, by appealing to first-order perturbation theory, the simple relationship

$$G'_\infty \frac{a^3}{kT} = \frac{3\phi}{4\pi} + \frac{3\phi^2}{40\pi} D_{\text{eff}}^4 g_{\text{hs}}(2; \phi_{\text{eff}}) F(D_{\text{eff}}) \quad [13]$$

is obtained for thin double layers, where $F(D_{\text{eff}}) = -d\Psi(r)/kT/dr|_{r=D_{\text{eff}}}$ is the force law evaluated at a dimensionless effective hard-sphere diameter: $D_{\text{eff}} = 2(\phi_{\text{eff}}/\phi)^{1/3}$. This effective hard-sphere diameter accounts for the extra excluded volume among particles due to their charged nature. Note that this expression differs significantly from previously derived formulas suited to ordered dispersions (23, 26, 28, 37). When the interaction potential is specified, the above formula is fully analytic since the hard-sphere radial distribution function at contact is related simply to the virial equation of state. We use the following form for the contact value of the hard-sphere radial distribution function:

$$g_{\text{hs}}(2; \phi) = \begin{cases} \dfrac{1 - \phi/2}{(1-\phi)^3} & 0 < \phi < 0.5 \\ \dfrac{1}{4\phi} \dfrac{1.21 + \phi}{0.64 - \phi} & 0.5 < \phi < 0.64. \end{cases} \quad [14]$$

For volume fractions below 0.5 this is the well-known Carnahan–Starling (53) expression, while above 0.5 the divergent form agrees with computer simulations of disordered hard-sphere dispersions (54).

The dispersions in this study are complicated multicomponent systems consisting of charged macroparticles with accompanying counter ions and added electrolyte. Despite this complexity, we describe these dispersions with a simple hard-sphere model. The model derived for the shear modulus (Eq. [13]) is based on the idea that the most important feature of the colloidal structure is the location of the first correlation peak in the radial distribution function. An effective hard-sphere radial distribution function is defined and parametrized by D_{eff}, the effective hard-sphere diameter. This effective hard-sphere structure is used to model the true structure of the charged-sphere system by shifting the $g_{\text{hs}}(r)$ a distance $D_{\text{eff}} - 2$, leading to a correspondence in peak position.

The effective hard-sphere diameter D_{eff} is defined here by mapping the divergence in the zero-shear viscosity onto that of hard spheres. Although alternative experimental methods exist (55, 56), as well as statistical mechanical treatments (57), a rheological method is chosen, as the mapping is being used for modeling rheological properties. The zero-shear viscosity of all the dispersions used here is well described in the concentrated regime by the phenomenological Quemada equation (58)

$$\eta_0/\mu = (1 - \phi/\phi_{\text{max}})^{-2}, \quad [15]$$

where ϕ_{max} is an effective maximum packing fraction. This relation has been used to model successfully both charged- (1) and hard-sphere dispersions (59–61) over large ranges of volume fraction. The maximum packing fraction is extracted from the linear high concentration asymptote of an $\eta_0^{-1/2}$ vs ϕ plot, as the intercept of the abscissa. The effective hard-sphere diameter (scaled by the particle radius a) is then identified from the scaling relation, $D_{\text{eff}} = 2(\phi_{\text{max}}^{\text{hs}}/\phi_{\text{max}})^{1/3}$, where $\phi_{\text{max}}^{\text{hs}}$ is the volume fraction at which the hard-sphere viscosity diverges. Although $\phi_{\text{max}}^{\text{hs}}$ is often taken as 0.64, the random close packing fraction, experiments on hard-sphere dispersions have shown that $\phi_{\text{max}}^{\text{hs}}$ lies in the range 0.58–0.64 (55, 56). We take $\phi_{\text{max}}^{\text{hs}} = 0.61$ in accordance with

Marshall and Zukoski (60). The zero-shear viscosities were extracted from well-defined Newtonian low-shear plateaus, an example of which is shown in Fig. 4, present in steady shear flow curves.

Once the effective hard-sphere diameter has been determined we can proceed with the evaluation of the surface charge from the shear modulus measurements. The interaction potential is substituted into the G'_∞ model (Eq. [13]). The result is a nonlinear equation for the surface charge because the inverse Debye length depends on the surface charge (see Eq. [8]). This effect is brought about because the number of counter ions in solution depends on the macroparticle charge through charge neutrality (1, 17, 62). As a consequence, the procedure for calculating the model G'_∞ is iterative, requiring initial estimates for the effective surface charge Q before G'_∞ can be calculated.

Since the surface charge is the only unknown parameter in the G'_∞ model, Q can in principle be extracted from a single G'_∞ measurement. To provide more confidence in the analysis we have measured G'_∞ for concentration series, obtained by diluting stock dispersions with electrolyte solution. As the surface charge is unknown a priori, the ionic strength cannot be kept constant with concentration. However, by diluting stock dispersions with the same electrolyte solution as dialyzed against, we find in our calculations only small ionic strength variations with particle concentration (κa varies by ~1% along a concentration series). The initial ionic strength and Debye length are calculated from the Donnan equilibrium (Eqs. [8] and [9]). Values for lower particle concentrations are calculated by accounting for the new electrolyte added and the change in effective solvent volume due to the dilution. All calculations are done assuming the surface charge does not change with particle concentration, an assumption supported by recent computer simulations (48).

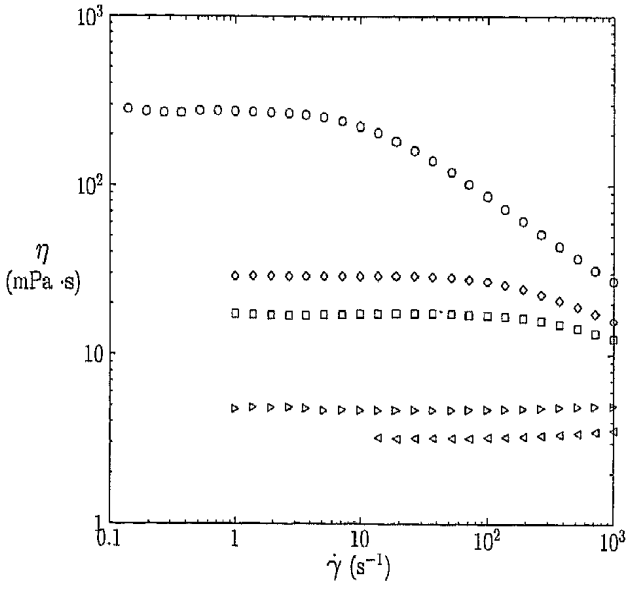

FIG. 4. Shear viscosity as a function of shear rate for PBMA/AA dispersions with a = 43.5 nm and [KCl] = 10 mM: (○) ϕ = 0.333, (◇) 0.311, (□) 0.296, (▷) 0.251, and (◁) 0.220.

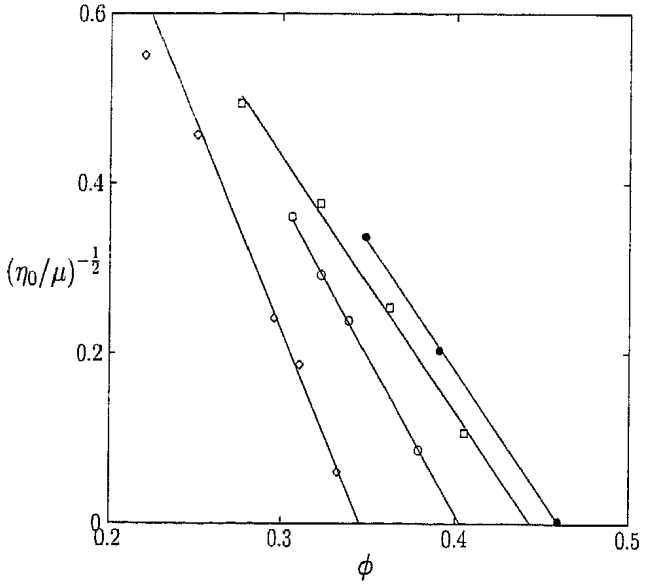

FIG. 5. Determination of effective maximum packing fraction for PBMA/AA dispersions with a = 43.5 nm. From left to right: [KCl] = 10, 25, 40, and 50 mM. The lines are linear least-squares fits to the terminal slopes of the data.

RESULTS AND DISCUSSION

To determine the surface charge from the effective hard-sphere model, the values of the effective hard-sphere diameter were extracted from the low-shear-viscosity plateaus as a function of particle concentration. Typical results are shown in Fig. 4 for PBMA/AA dispersions at [KCl] = 10 mM. Figure 5 shows an example of the plots used to extract the effective maximum packing fraction and the effective hard-sphere diameter for the PBMA/AA dispersions. As seen, the effective maximum packing fraction increases with increasing ionic strength, consistent with increasing amounts of added salt leading to stronger screening of the particle interactions. The maximum packing fractions and the resulting effective hard-sphere diameters are tabulated in Table 2.

The torsional resonator supplies, in addition to the shear modulus, the high-frequency viscosity of the dispersions. The data for the PBMA/AA dispersions are shown in Fig. 6 as functions of the dialysate ionic strength. The high-frequency viscosity is seen to increase rather strongly with decreasing ionic strength. At higher ionic strengths the data appear to superpose. All the data sets show deviations from hard-sphere behavior as given by Eq. [6]. To correlate these high-frequency viscosities, we employ the effective hard-sphere scaling as derived from the zero-shear viscosity. Shown in Fig. 7 are the η'_∞ for the PBMA and PBMA/AA dispersions as functions of the effective hard-sphere volume fraction $\phi_{\text{eff}} = \phi(D_{\text{eff}}/2)^3$. The hard-sphere scaling serves reasonably well to reduce the high-frequency viscosity data

TABLE 2

Summary of Results: Particle Type, Radius, Dialysate Ionic Strength, Weight Percentage Initiator, Effective Surface Charge Density, Maximum Packing Volume Fraction, Effective Hard-Sphere Diameter, and Reciprocal Debye Length

Particle type	a (nm)	[KCl] (mM)	NaPS (wt%)	q (μC/cm^2)	ϕ_{max}	D_{eff}	κa
PBMA1	38	10	0.40	0.99	0.359	2.387	12.7
PBMA2	37	30	0.15	2.14	0.408	2.287	21.4
PBMA1	38	30	0.40	2.09	0.410	2.283	22.0
PBMA3	40	30	0.67	2.72	0.410	2.282	23.2
PBMA1	38	50	0.40	2.55	0.451	2.212	28.3
PBMA/AA	43.5	10	0.40	1.25	0.346	2.415	14.7
PBMA/AA	43.5	25	0.40	2.76	0.403	2.297	23.1
PBMA/AA	43.5	40	0.40	3.31	0.443	2.224	29.1
PBMA/AA	43.5	50	0.40	3.44	0.460	2.197	32.6

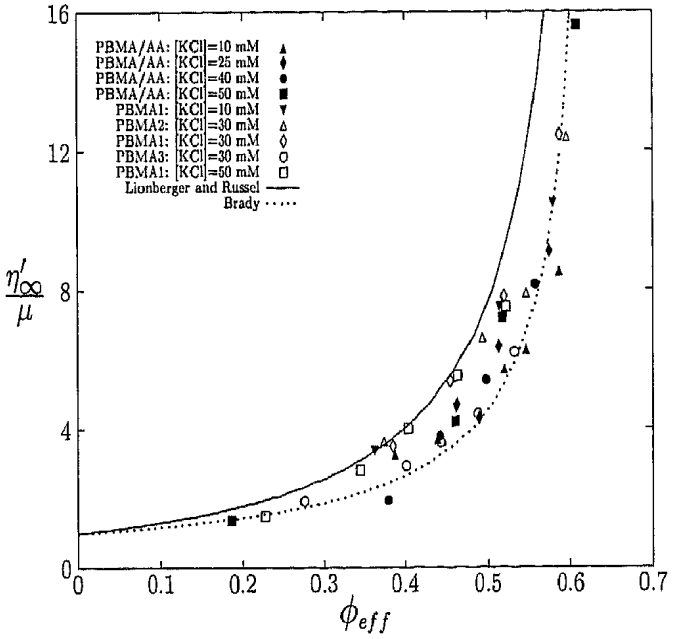

FIG. 7. High-frequency viscosity as a function of effective hard-sphere volume fraction $\phi_{eff} = \phi(D_{eff}/2)^3$, as labeled. The lines represent different hard-sphere predictions.

to a master curve. Hence, it should be possible to use the high-frequency viscosity in the determination of the effective hard-sphere diameter, eliminating the need for the zero-shear viscosity measurements. The zero-shear viscosities are, however, orders of magnitude larger than the corresponding high-frequency viscosities and provide a more reliable database from which to extrapolate. Figure 7 also shows two hard-sphere predictions, one due to Lionberger and Russel (44) (see Eq. [6]) and the other,

$$\eta'_\infty/\mu = (1 - \phi/0.64)^{-1}, \qquad [16]$$

due to Brady (51). The experimental data lie between the predictions of the two models.

Figure 8 shows the shear moduli derived from the Rheoswing measurements for the PBMA/AA dispersions for varying particle volume fraction and ionic strength. The shear modulus is seen to increase with increasing concentration and decreasing ionic strength. These trends are also observed for the PBMA systems and for ordered dispersions studied by others (17–19). The lines shown in Fig. 8 are least-squares representations of the effective hard-sphere model. We find that the model is able to reproduce the data.

As the surface charge is the only unknown quantity in the G'_∞ model, the others being determined independently or calculated internally in a consistent manner, it can be ex-

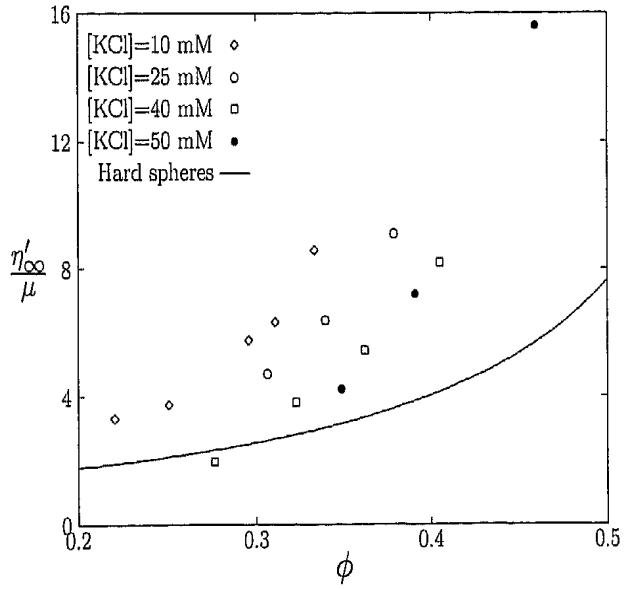

FIG. 6. High-frequency viscosity for PBMA/AA dispersions as a function of volume fraction and ionic strength. The line represents hard-sphere behavior (44).

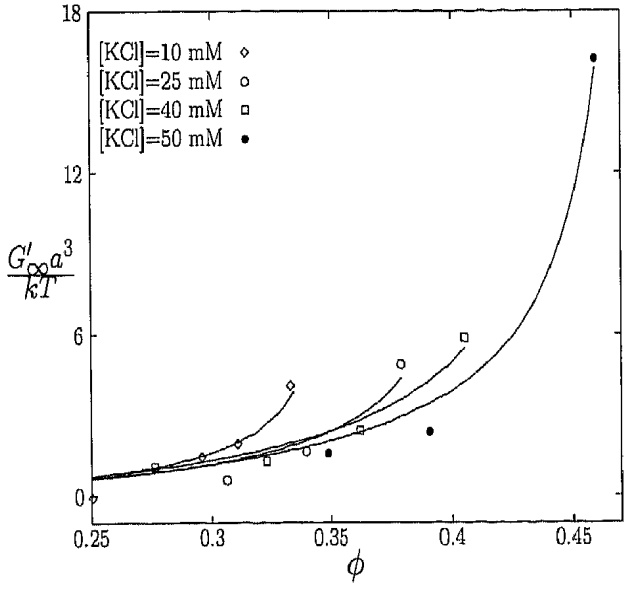

FIG. 8. Dimensionless high-frequency shear modulus as a function of the volume fraction for the PBMA/AA dispersions. The lines represent least-squares fits of the effective hard-sphere model.

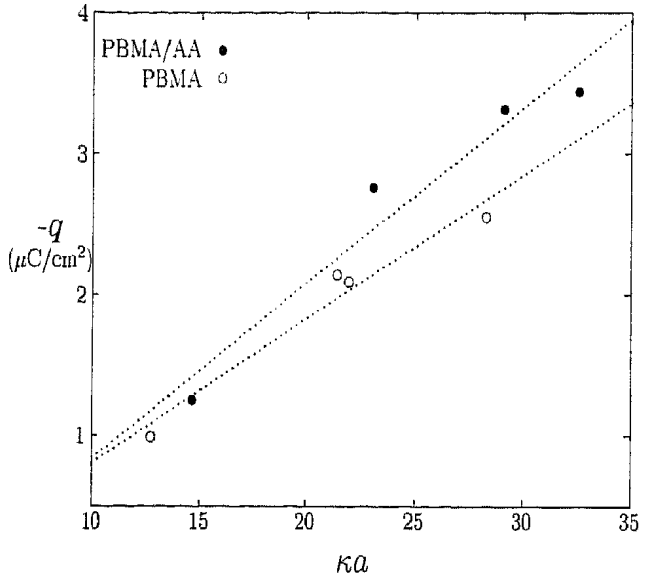

FIG. 9. Surface charge density vs reciprocal Debye length for PBMA/AA and PBMA dispersions. The lines are linear least-squares fits to the data sets, yielding surface potentials of $\Psi_S = -78$ mV for PBMA/AA and $\Psi_S = -56$ mV for PBMA.

tracted as a function of the ionic strength. In Fig. 9 the surface charge density is shown as a function of the reciprocal Debye length for the PBMA/AA and PBMA dispersions. There it can be seen that the effective surface charge increases with ionic strength or κa. This is the expected trend for particles with weak acid surface groups and is a consequence of the surface equilibrium (63); at higher ionic strengths the added electrolyte provides a stronger screening in the ionic medium, leading to a higher degree of surface dissociation. As seen in Fig. 9 we observe a similar trend for the PBMA dispersions which contain only strong acid surface groups. At the pH at which these experiments were conducted (pH 6) surface equilibrium is not expected to influence the charge for these strong acid PBMA dispersions, but an increasing charge density is nevertheless observed. The fact that the surface charge densities for the PBMA dispersions are generally lower than those for the PBMA/AA is reassuring in light of the analytical charge found from conductometric titration. As seen in Table 1 the titrated charge for the PBMA/AA dispersions exceed those of the PBMA dispersions by an order of magnitude due to the presence of the weak acid surface groups derived from the added acrylic acid (AA).

To understand the ionic strength dependence of the PBMA surface charge it is necessary to realize that the surface charge should be renormalized. This follows from the use of the linear Poisson–Boltzmann theory in the model for the interaction potential. The concept of a renormalized charge can be viewed physically as a result of counter ion condensation; the counter ions are located in a thin layer around the particle, causing a lowering of the electrostatic potential near the sphere surface (13–15). The renormalization serves to simplify the theoretical considerations in the analysis of experimental data. It carries with it the penalty that the surface charge obtained is not the actual bare surface charge, but a smaller effective surface charge, reflecting the charged particle plus some recondensed counter ions (15). For colloidal crystals, Alexander *et al.* (13) developed a procedure, based on the Poisson–Boltzmann cell model, for converting the renormalized charge to the bare surface charge. For the purpose of this study, it suffices to know that such conversion procedures exist. We are in fact more interested in the renormalized, effective surface charge, as this quantity can be used directly to predict phase behavior (64), colloidal structure (10, 63), and dynamics (5, 12). The effective charge has been found, both numerically (13) and by computer simulations (48), to be an increasing function of the dispersion ionic strength, even though the bare charge is kept fixed. The PBMA data in Fig. 9 provides experimental support for this property of the effective charge.

As seen in Fig. 9, the charge is roughly a linear function of κa. The lines shown are linear least-squares fits to the data, the slopes of which yield the surface potential according to the Debye–Hückel formula

$$Q\frac{L_B}{a} = (1 + \kappa a)\frac{e\Psi_S}{kT}. \qquad [17]$$

The linearity of the data in Fig. 9 implies that the surface potential Ψ_S remains independent of the electrolyte level in the regime investigated. We obtain $\Psi_S = -78$ and -56 mV for the PBMA/AA and PBMA dispersions, respectively. These values are in good agreement with $\zeta = -68$ mV obtained from Henry's equation (1, 38) applied to the electrophoretic mobility of the PBMA/AA dispersions. Similar increasing trends of the electrophoretic charge with ionic strength were observed by Midmore and Hunter (65).

In Fig. 9 the data partition themselves onto two lines according to whether the particles contain added weak acid groups or only a smaller number of strong acid groups. The exception is PBMA3 at [KCl] = 30 mM (see Table 2), which superposes on the PBMA/AA data. This dispersion was synthesized with a higher initiator content. Increasing the amount of initiator is an effective means, in the case of PBMA, of incorporating more strong surface acid groups (66). The resulting titration charge in Table 1 shows indeed that PBMA3 has a higher surface charge than either PBMA1 or PBMA2, both of which were synthesized using lower initiator contents. The effective charge density of the PBMA/AA dispersions is found to be an order of magnitude smaller than the corresponding titrated charge (see Table 1), a well-documented effect (13, 16, 65). The PBMA dispersions show effective charge densities that increase with increasing initiator content, in agreement with, but somewhat

larger than, the titration measurements. The fact that the present method operates at high particle concentrations and can consistently distinguish between dispersions with different charge densities not only serves to validate the method itself, but also shows that the renormalized charge concept holds at high colloid concentrations and high ionic strengths.

CONCLUSION

A method for determining the effective surface charge density directly in concentrated liquid charge-stabilized dispersions has been demonstrated. Measurements of the high-frequency limiting shear modulus as a function of added electrolyte and surface acid content show sensitivity to the strength and range of the interparticle interaction and are thus well suited to probing the strength of colloidal forces. A hard-sphere perturbation theory of the dispersion microstructure yields, for high ionic strengths, a simple relationship between the high-frequency shear modulus and the effective surface charge. The only input is an effective hard-sphere diameter, determined in this work from the high concentration behavior of the zero-shear viscosity. The resulting effective charge is found to show the proper dependence on electrolyte concentration and surface acid content. The extracted charge densities agree well with dilute measurements of the electrophoretic mobility, provided these are analyzed in a consistent manner (linear Poisson–Boltzmann theory). These findings suggest that the diffuse double-layer charge remains essentially constant with particle concentration but is an increasing function of added electrolyte. Finally, because the method is, in general, not specific to electrostatically stabilized dispersions, it could be used to characterize other methods of stabilizing colloidal particles, such as polymer steric stabilization.

APPENDIX

Approximate Formula for the Elastic Shear Modulus

Simple analytical expressions relating the high-frequency elastic shear modulus to the interaction potential have been derived for systems in which the structure is highly localized. For liquids the structure is no longer localized, rendering these formulas inappropriate. We pursue a simple analytic relationship between the high-frequency shear modulus and the interaction potential for molecular liquids or, equivalently, a monodisperse liquid dispersion in the absence of hydrodynamic particle interactions.

When the interaction potential is rapidly decaying, the Zwanzig and Mountain formula can be integrated by parts, leading to

$$G'_\infty \frac{a^3}{kT} = \frac{3\phi}{4\pi} - \frac{3\phi^2}{40\pi}\int_0^\infty dr r^4 \frac{dg(r)}{dr}\frac{d\Psi(r)/kT}{dr}. \quad [18]$$

A direct hard-sphere mapping is ill suited to treating the above expression because the shear modulus of the hard-sphere reference system is infinite (44, 67). We appeal instead to perturbation theory in making the substitution

$$g(r;\phi) \approx g_{hs}(2r/D_{eff};\phi_{eff}). \quad [19]$$

In this approximation the implicit dependence of $g(r)$ on the interaction potential is described through an effective hard-sphere diameter $D_{eff} = 2(\phi_{eff}/\phi)^{1/3}$. The approximate $g_{hs}(r)$ has been shifted radially by an amount $D_{eff} - 2$ to capture the effect of the additional excluded volume due to, in this case, the electrostatic repulsion between the colloidal particles. To obtain an analytic approximation we explicitly factor out the discontinuity in the hard-sphere radial distribution function by writing it as a product of the Boltzmann factor and the continuous, so-called cavity correlation function $y(r)$. Noting that the Boltzmann factor for hard spheres is just a unit step function, we arrive at the identity

$$g_{hs}(2r/D_{eff};\phi_{eff}) = y_{hs}(2r/D_{eff};\phi_{eff})U(r - D_{eff}). \quad [20]$$

Substitution into Eq. [18] results in

$$G'_\infty \frac{a^3}{kT} = \frac{3\phi}{4\pi} - \frac{3\phi^2}{40\pi} D_{eff}^4 y_{hs}(2;\phi_{eff}) \left.\frac{d\Psi(r)/kT}{dr}\right|_{r=D_{eff}} - \frac{3\phi^2}{40\pi}\int_0^\infty dr r^4 \frac{dy_{hs}(2r/D_{eff})}{dr}\frac{d\Psi(r)/kT}{dr}. \quad [21]$$

When the interaction potential is of short range the integral in the above contributes little. Neglecting this term can be viewed as a short-range approximation to Eq. [21], which, after evaluation of $y_{hs}(2;\phi_{eff})$, becomes

$$G'_\infty \frac{a^3}{kT} = \frac{3\phi}{4\pi} - \frac{3\phi^2}{40\pi} D_{eff}^4 g_{hs}(2;\phi_{eff}) \left.\frac{d\Psi(r)/kT}{dr}\right|_{r=D_{eff}}. \quad [22]$$

This formula is fully analytic when one of the available hard-sphere theories for $g_{hs}(2)$ is used. Note that previously derived G' models for crystalline dispersions use a delta function representation of the structure, whereas we take full account of $g(r)$ in deriving Eq. [22] and instead approximate the integral appearing in the Zwanzig and Mountain formula.

ACKNOWLEDGMENTS

We thank Dr. S. Vogt for kindly performing the electrophoretic mobility measurements and Dr. R. Balk for determining the titration charges.

REFERENCES

1. Russel, W. B., Saville, D. A., and Schowalter, W. R., "Colloidal Dispersions." Cambridge, New York, 1989.
2. Robbins, M. O., Kremer, K., and Grest, G. S., *J. Chem. Phys.* **88,** 3286 (1988).
3. Monovoukas, Y., and Gast, A. P., *J. Colloid Interface Sci.* **128,** 533 (1989).
4. Pusey, P. N., *in* "Liquids, Freezing and Glass Transition" (J.-P. Hansen, D. Levesque, and J. Zinn-Justin, Eds.). North-Holland, Amsterdam, 1991.
5. Nägele, G., *Phys. Rep.* **272,** 215 (1996).
6. Hunter, R. J., "Zeta Potential in Colloid Science." Academic Press, New York, 1981.
7. O'Brien, R. W., *J. Colloid Interface Sci.* **92,** 204 (1983).
8. O'Brien, R. W., Cannon, D. W., and Rowlands, W. N., *J. Colloid Interface Sci.* **173,** 406 (1995).
9. Wagner, N. J., Krause, R., Rennie, A. R., D'Aguanno, B., and Goodwin, J. W., *J. Chem. Phys.* **95,** 494 (1991).
10. Härtl, W., Versmold, H., and Wittig, U., *Langmuir* **8,** 2885 (1992).
11. Deggelmann, M., Palberg, T., Hagenbüchle, M., Maier, E. E., Krause, R., Graf, C., and Weber, R., *J. Colloid Interface Sci.* **143,** 318 (1991).
12. Bitzer, F., Palberg, T., Löwen, H., Simon, R., and Leiderer, P., *Phys. Rev. E* **50,** 2821 (1994).
13. Alexander, S., Chaikin, P. M., Grant, P., Morales, G. J., Pincus, P., and Hone, D., *J. Chem. Phys.* **80,** 5776 (1984).
14. Belloni, L., *J. Chem. Phys.* **85,** 519 (1986).
15. Kjellander, R., and Mitchell, D. J., *Chem. Phys. Lett.* **200,** 76 (1992).
16. Crocker, J. C., and Grier, D. G., *Phys. Rev. Lett.* **73,** 352 (1994).
17. Lindsay, H. M., and Chaikin, P. M., *J. Chem. Phys.* **76,** 3774 (1982).
18. Benzing, D. W., and Russel, W. B., *J. Colloid Interface Sci.* **83,** 178 (1981).
19. Buscall, R., Goodwin, J. W., Hawkins, M. W., Ottewill, R. H., *J. Chem. Soc., Faraday Trans. 1* **78,** 2873 (1982).
20. Goodwin, J. W., Gregory, T., and Stile, J. A., *Adv. Colloid Interface Sci.* **17,** 185 (1982).
21. Goodwin, J. W., Gregory, T., Miles, J. A., and Warren, B. C. H., *J. Colloid Interface Sci.* **97,** 488 (1984).
22. Goodwin, J. W., Hughes, R. W., Partridge, S. J., and Zukoski, C. F., *J. Chem. Phys.* **85,** 559 (1986).
23. Evans, I. D., and Lips, A., *J. Chem. Soc., Faraday Trans.* **86,** 3413 (1990).
24. Raynaud, L., Ernst, B., Vege, C., and Mewis, J., *J. Colloid Interface Sci.* **181,** 11 (1996).
25. Zwanzig, R., and Mountain, R. D., *J. Chem. Phys.* **43,** 4464 (1965).
26. Wagner, N. J., *J. Colloid Interface Sci.* **161,** 169 (1993).
27. Chen, L.-B., and Zukoski, C. F., *J. Chem. Soc., Faraday Trans.* **86,** 2629 (1990).
28. Buscall, R., *J. Chem. Soc., Faraday Trans.* **87,** 1365 (1991).
29. van der Vorst, B., van den Ende, D., and Mellema, J., *Physica B* **228,** 180 (1996).
30. de Rooij, R., van den Ende, D., Duits, M. H. G., and Mellema, J., *Phys. Rev. E* **49,** 3038 (1994).
31. Mitaku, S., Ohtsuki, T., Enari, K., Kishimoto, A., and Okano, K., *Jap. J. Appl. Phys.* **17,** 305 (1978).
32. Palberg, T., Kottal, J., Loga, T., Hecht, H., Simnacher, E., Falcoz, F., and Leiderer, P., *J. Phys. III* **4,** 457 (1994).
33. van der Werff, J. C., de Kruif, C. G., Blom, C., and Mellema, J., *Phys. Rev. A* **39,** 795 (1989).
34. Woutersen, A. T. J. M., Mellema, J., Blom, C., and de Kruif, C. G., *J. Chem. Phys.* **101,** 542 (1994).
35. Mason, W. P., *Trans. A. S. M. E.* **69,** 359 (1947).
36. Ferry, J. D., "Viscoelastic Properties of Polymers." Wiley, New York, 1980.
37. Joanny, J. F., *J. Colloid Interface Sci.* **71,** 622 (1979).
38. Henry, D. C., *Proc. Royal Soc. A* **133,** 106 (1931).
39. Frith, W. J., Strivens, T. A., and Mewis, J., *J. Colloid Interface Sci.* **139,** 55 (1990).
40. Yoshizaki, H., *Polymer J.* **25,** 553 (1993).
41. Schrag, J. L., and Johnson, M. J., *Rev. Sci. Instr.* **42,** 224 (1971).
42. Blom, C., and Mellema, J., *Rheol. ACTA* **23,** 98 (1984).
43. van den Ende, D., Mellema, J., and Blom, C., *Rheol. ACTA* **31,** 194 (1992).
44. Lionberger, R. A., and Russel, W. B., *J. Rheology* **38,** 1885 (1994).
45. Lionberger, R. A., and Russel, W. B., *J. Rheology* **41,** 399 (1997).
46. Bell, G. M., Levine, S., and McCartney, L. N., *J. Colloid Interface Sci.* **33,** 335 (1970).
47. Russel, W. B., and Benzing, D. W., *J. Colloid Interface Sci.* **83,** 163 (1981).
48. Stevens, M. J., Falk, M. L., and Robbins, M. O., *J. Chem. Phys.* **104,** 5209 (1996).
49. Hiemenz, P. C., "Principles of Colloid and Surface Chemistry." Dekker, New York, 1977.
50. Verwey, E. J. W., and Overbeek, J. G., "Theory of the Stability of Lyophobic Colloids." Elsevier, Amsterdam, 1948.
51. Brady, J. F., *J. Chem. Phys.* **99,** 567 (1993).
52. Bossis, G., Brady, J. F., and Mathis, C., *J. Colloid Interface Sci.* **126,** 1 (1988).
53. Carnahan, N. F., and Starling, K. E., *J. Chem. Phys.* **51,** 635 (1969).
54. Woodcock, L. V., *Ann. New York Acad. Sci.* **371,** 274 (1981).
55. Phan, S.-E., Russel, W. B., Cheng, Z., Zhu, J., Chaikin, P. M., Dunsmuir, J. H., and Ottewill, R. H., *Phys. Rev. E* **54,** 6633 (1996).
56. Meeker, S. P., Poon, W. C. K., and Pusey, P. N., *Phys. Rev. E* **55,** 5718 (1997).
57. van Megen, W., and Snook, I., *J. Colloid Interface Sci.* **100,** 359 (1984).
58. Quemada, D., *Rheol. ACTA* **16,** 82 (1977).
59. de Kruif, C. G., van Iersel, E. M. F., Vrij, A., and Russel, W. B., *J. Chem. Phys.* **83,** 4717 (1986).
60. Marshall, L., and Zukoski, C. F., *J. Phys. Chem.* **94,** 1164 (1990).
61. Jones, D. A. R., Leary, B., and Boger, D. V., *J. Colloid Interface Sci.* **147,** 479 (1991).
62. Beresford-Smith, B., Chan, D. Y. C., and Mitchell, D. J., *J. Colloid Interface Sci.* **105,** 216 (1985).
63. Gisler, T., Schulz, S. F., Borkovec, M., Sticher, H., Schurtenberger, P., D'Aguanno, B., and Klein, R., *J. Chem. Phys.* **101,** 9924 (1994).
64. Palberg, T., Mönch, W., Bitzer, W., Piazza, R., and Bellini, T., *Phys. Rev. Lett.* **74,** 4555 (1995).
65. Midmore, B. R., and Hunter, R. J., *J. Colloid Interface Sci.* **122,** 521 (1988).
66. Davies, M. C., Lynn, R. A. P., Davis, S. S., Hearn, J., Watts, J. F., Vickerman, J. C., and Johnson, D., *J. Colloid Interface Sci.* **156,** 229 (1993).
67. Heyes, D. M., and Aston, P. J., *J. Chem. Phys.* **99,** 567 (1994).
68. Zwetsloot, J. P. H., and Leyte, J. C., *J. Colloid Interface Sci.* **163,** 362 (1994).
69. Yamanaka, J., and Ise, N., *J. Colloid Interface Sci.* **179,** 324 (1996).